JOURNAL OF SOLID STATE CHEMISTRY 30, 299–310 (1979)

Vacancy Contents and Phase Equilibria of Ti-Substituted MnZn Ferrite

D. W. JOHNSON, JR., P. K. GALLAGHER, M. F. YAN, AND H. SCHREIBER

Bell Laboratories, Murray Hill, New Jersey 07974

Received August 14, 1978; in revised form January 22, 1979

Measurement of the divalent iron content in acid dissolved MnZn ferrites, fired in controlled atmospheres at various temperatures and quenched, allows calculation of cation vacancy contents. Addition of Ti^{4+} to these ferrites resulted in the introduction of vacancies at the rate of about 0 to 0.3 per Ti^{4+} depending on heat treatment conditions. Data are presented whereby the vacancy content with Ti^{4+} can be calculated based on the oxygen content of the undoped ferrite as available in the literature. Ti^{4+} stabilizes the hexagonal hematite-like structure and the phase boundary is presented as a function of Ti^{4+} and temperature. The vacancy contents at the phase boundary in Ti^{4+}-doped ferrite as a function of temperature are in agreement with those calculated from the literature for undoped MnZn ferrites. Finally, the total oxygen content of coexisting spinel and hexagonal phases is presented.

Introduction

It is well known that addition of titanium to MnZn ferrites results in the formation of divalent iron (Fe^{2+}) which in turn can control the permeability vs temperature through its effect on the magnetocrystalline anisotrophy constant, K_1 (*1–6*). The addition of TiO_2 into the spinel lattice also has the effect of creating divalent iron, vacancies, or both. the limiting cases for TiO_2 dissolution in ferrite are:

$$(TiO_2)_{rutile} \rightarrow (Ti^{4+} + 2O^{2-} + \tfrac{1}{2}V_c)_{spinel}, \quad (1)$$

where only cation vacancies are formed, and

$$(TiO_2)_{rutile} + (\tfrac{4}{3}Fe^{3+})_{spinel} \rightarrow (Ti^{4+} + \tfrac{4}{3}Fe^{2+} + \tfrac{4}{3}O^{2-})_{spinel} + \tfrac{1}{3}(O_2)\uparrow, \quad (2)$$

where no vacancies are formed but enough trivalent iron is reduced to charge compensate the Ti^{4+} in the spinel lattice.

In recent studies (*7*) showing a marked enhancement of grain growth rates in the presence of Ti^{4+} it was hypothesized that Ti^{4+} did introduce cation vacancies which lead to increased pore mobility by enhancing the diffusion of cations displaced by an advancing pore. The simultaneous transport of anions was assumed to be by a rapid gas phase transport across the pore. Enhanced pore mobility would, in turn, lead to enhanced grain boundary mobility for boundaries with attached pores. Justification for assuming an increased vacancy content with Ti^{4+} was made (*7*) based on the argument that Eq. (2) with no vacancy increase leads to an increased ratio $[Fe^{2+}]/[Fe^{3+}]$. However, the equilibrium oxidation–reduction for iron requires, in the absence of any other changes, an *increase* in cation vacancies with an increase in $[Fe^{2+}]/[Fe^{3+}]$. Thus, it was concluded that Ti^{4+} must lead to some increase in the cation vacancy content but no quantitative data were available. The lack of such quantitative

0022-4596/79/120299-12$02.00/0

data on cation vacancy concentration as a function of Ti^{4+} for use in calculating pore mobilities leads to the present study. However, information on vacancy concentration in Ti-doped MnZn ferrites is also valuable in tailoring ferrites for applications in which the disaccommodation behavior is important. Disaccommodation in MnZn ferrites is recognized to be related to the diffusion rates of cations and cation vacancies (*8–11*). As the total iron content increases, or the sintering atmosphere becomes more oxidizing, the cation vacancy content increases and the disaccommodation increases or the disaccommodation spectrum changes (*11–14*). While the actual mechanism of disaccommodation is not completely understood, phenomenological observations referred to above support the hypothesis that cation vacancies play a critical role by increasing cation diffusion rates. This diffusion leads to a local induced anisotropy which stabilizes domain walls.

To summarize the importance of the effect of additives such as Ti on the vacancy concentration and oxidation state of iron as a function of firing conditions, the following should be considered. (1) The vacancy content affects densification and grain growth kinetics. (2) In tailoring magnetic properties, additives such as Ti^{4+} can be used to introduce Fe^{2+} which in turn changes the permeability–temperature spectrum. (3) Introduction of vacancies and Fe^{2+} with additives such as Ti^{4+} affects the disaccommodation temperature spectrum and loss characteristics.

Magnetic and other physical properties of ferrites have often been measured as a function of firing and annealing conditions designed to set the $[Fe^{2+}]/[Fe^{3+}]$ ratio and thus set the cation vacancy content. Iida (*15*) prepared ferrites with a uniform density of cation vacancies by a sealed quartz tube technique and discussed how the vacancy content affects the magnetic relaxation. The actual weight percentage of Fe^{2+} in MnZn ferrites as a function of temperature and oxygen partial pressure has been measured by Slick (*16*) and Morineau and Paulus (*17*). The data from these studies allow the calculation of the vacancy content for the undoped ferrites. Morineau (*18*) has further refined thermogravimetric data on MnZn ferrites using site preferences for cations to develop a model of oxidation–reduction equilibria.

Hanke (*19*) and Hanke and Zenger (*20*) have studied the effects of Ti^{4+} and Sn^{4+} on the magnetic properties of MnZn ferrite. They have confirmed the effect of these additions on the magnetocrystalline anisotropy as discussed earlier. Hanke (*19*) has also measured the divalent iron content as a function of the amount of Ti^{4+}. It was found that each Ti^{4+} substituted for a divalent Mn or Zn reduced two Fe^{3+} to Fe^{2+}. This, of course, implies an increase in the $[Fe^{2+}]/[Fe^{3+}]$ without an increase in the number of cation vacancies. As reviewed earlier, this is inconsistent with equilibrium thermodynamic arguments but may be approximately true for ferrite samples fired in relatively reducing conditions where cation vacancy concentrations are always low.

Thus, while the importance of cation vacancies in ferrites is recognized, little work has been done to actually measure the concentration of cation vacancies with additions of dopants such as Ti. This work serves to fill that gap with quantitative data showing vacancy contents for MnZn ferrites as a function of Ti content, firing temperature, and firing atmosphere. As side benefits of this study, the phase boundary between the spinel phase and the hematite-type phase has been delineated as a function of Ti content, and the stoichiometry of the hexagonal and spinel phases in equilibrium has been calculated.

This work was carried out using a single MnZn ferrite composition to which controlled additions of Ti^{4+} were made. The

general spinel formula for these ferrites is:

$$M^{2+}Fe_k^{2+}Fe_{2-k}^{3+}Ti_x^{4+}V_\alpha O_{4+\beta}, \qquad (3)$$

where M^{2+} is Mn^{2+}, Zn^{2+} as well as Fe^{2+} for excess iron ferrites; k is the excess Fe^{2+} generated either by the addition of Ti^{4+} or by reducing conditions (note that k can be negative if some of the Fe^{2+} in M^{2+} is oxidized); x is the amount of Ti^{4+} dissolved per formula unit; α is the number of cation vacancies per formula unit; and β is the excess oxygen per formula unit.

Note that as Ti^{4+} is added ($x > 0$), the total number of cations in the formula unit exceeds 3. This representation is used to avoid the clumsy normalization which would be needed to maintain the conventional M_3O_4 spinel formula when Ti^{4+} is added rather than substituted for some other ion.

The excess divalent iron, k, is calculated from the measured wt% Fe^{2+} by:

$$k \simeq \frac{\text{wt fraction } Fe^{2+} \times \text{molecular wt of ferrite}}{55.85} - a, \qquad (4)$$

where a is the amount of total iron in excess of 2 in the spinel formula.

Examining expression (3), the cation–anion balance gives $\beta = \frac{4}{3}(\alpha + x)$ and the charge balance[1] gives $\beta = 2x - k/2$. Combining these gives:

$$\alpha = \frac{x}{2} - \frac{3}{8}k. \qquad (5)$$

Thus, knowing x and measuring k the cation vacancy concentration can be calculated.

Note that in expression (3) and throughout this study, the notation is designed to exclude Mn^{3+} in the presence of Fe^{2+}. This is convenient in that the divalent iron analyses described later employ the dissolution of the ferrites. The oxidation potentials for Mn^{3+} and Fe^{2+} in solution (*21*) push the aqueous equilibria strongly in favor of Fe^{2+} at room temperature. Thus, what is actually measured and reported as the Fe^{2+} content is the actual Fe^{2+} minus the Mn^{3+} content in the solid state ferrite.

The question of what is the distribution of Fe^{2+} and Mn^{3+} in the solid state ferrite has been argued elsewhere. Lotgering and Van Diepen (*22*) using Mössbauer spectroscopy have found that Mn^{3+} is unstable in the presence of Fe^{2+}. Other investigators (*6, 16, 23*), by measurement or assumption, have worked under a model where there is negligible Mn^{3+} where Fe^{2+} is present. On the other hand, Morineau (*18*) asserts that a significant fraction of the manganese in Mn–Zn ferrites is trivalent. Finally, Walz and Rivas (*24*) hypothesize $Mn^{3+}Fe^{2+}$ pairs to explain magnetic aftereffects in ferrites.

Experimental

This study was carried out on a single MnZn ferrite composition made by freeze-drying the appropriate reagent-grade sulfates. The analyzed cationic composition of this ferrite using the Coprex technique (*25*) (X-ray fluorescence) was:

$$Mn_{0.515}Zn_{0.397}Fe_{2.089}O_{4+\beta}.$$

A separate analyzed solution of Ti was made by dissolving tetramethyltitanate, $(CH_3O)_4Ti$, in a water–sulfuric acid mixture. Appropriate amounts of this solution were added to sublots of the Mn–Zn–Fe sulfate solution to give compositions with $x =$ 0.0125, 0.025, 0.05, and 0.1 using the notation in expression (3). These solutions were frozen and freeze-dried using the technique of Schnettler *et al.* (*26*). The freeze-dried sulfates were decomposed and calcined at 1000°C for 16 hr in a flowing nitrogen atmosphere.

[1] It is assumed that the cation vacancies in this structure are uncharged. This assumption is true in γ-Fe_2O_3 where there are large numbers of uncharged cation vacancies in the spinel structure. Also the spinel structure has many unfilled tetrahedral and octahedral sites which are apparently uncharged and which must be energetically similar to a cation vacancy.

Small pellets of the freeze-dried ferrite were pressed lightly at 14 MPa (2000 psi), giving green densities of about 1.8 g/cm^3. These were fired in open Pt containers by heating at 400°C/hr to temperatures ranging from 1200 to 1350°C in atmospheres of O_2–N_2 mixtures ranging from N_2 to 100% O_2 for times from 5 to 24 hr. The shorter times were used at the lowest O_2 atmospheres to prevent excessive Zn volatilization. At the completion of the heat treatment, the pellets were quenched in water. Experiments to compare air, water, liquid nitrogen, and both hydrocarbon and silicone oils as quenching media showed the water to give the most consistent Fe^{2+} analyses and best avoid reduction of the surface during quenching. Quenching rates are estimated to be $>10^3$ °C/sec. The loose packing of the powder resulted in low fired densities (3.3 to 4.0 g/cm^3) and thus aided in the equilibration of the ferrite with the furnace atmosphere.

Divalent iron analyses were done in triplicate using a coulometric titration technique described elsewhere (*27*).

Examination of the phases present was done by optical microscopy of polished sections and by X-ray diffraction. Quantitative chemical analyses of the phases present was done using an ETEC electron microprobe. Measurement of the relative volumes of phases in multiphase samples was done by the point counting method (*28*) using optical photomicrographs. Corrections were made for porosity by counting the volume fraction of pores in a like manner. At least 1000 random points were counted over a least seven micrographs for each determination.

Results and Discussion

(*a*) *Vacancy contents vs Ti^{4+} concentrations*

The wt% Fe^{2+} as a function of Ti concentration is shown in Fig. 1 for the samples

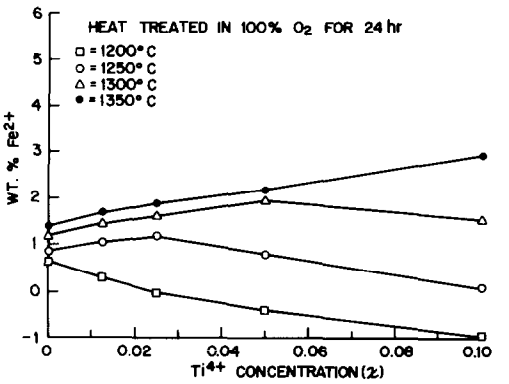

FIG. 1. Divalent iron content (wt% Fe^{2+} based on the total oxide weight) as a function of the Ti^{4+} added to a $M_3O_{4+\beta}$ spinel.

annealed in O_2. This example illustrates at 1350°C the expected trend of increasing Fe^{2+} with increasing Ti^{4+}. However, at 1250 and 1300°C the Fe^{2+} increases with Ti^{4+} to a point and then decreases thereafter. At the lowest temperature, 1200°C, any addition of Ti^{4+} to the ferrite reduces the total Fe^{2+} content. This unexpected behavior is related to the coexistence of a hexagonal hematite-like phase to be discussed in detail in the next section.

To discuss the effect of Ti^{4+} on the vacancy content, only those samples which were single-phase ferrite will be considered. Results of divalent iron analyses as exemplified in Fig. 1 were used to calculate k (Eq. (4)) and then α using Eq. (5). The results for all temperatures and atmospheres are shown in Figs. 2a–d. As expected, for a given atmosphere, the number of cation vacancies decreases with increasing temperature. Also, for a constant temperature, the number of vacancies increases with increasing oxygen content in the atmosphere.[2] The negative values of α for the nitrogen firings could represent some anion vacancies but it is more likely that the large measured amounts of

[2] The samples fired in nitrogen (Fig. 2d) had some exposure to oxygen due to system leaks, diffusion through the muffle, etc. It is estimated that the actual p_{O_2} was between 100 and 1000 ppm.

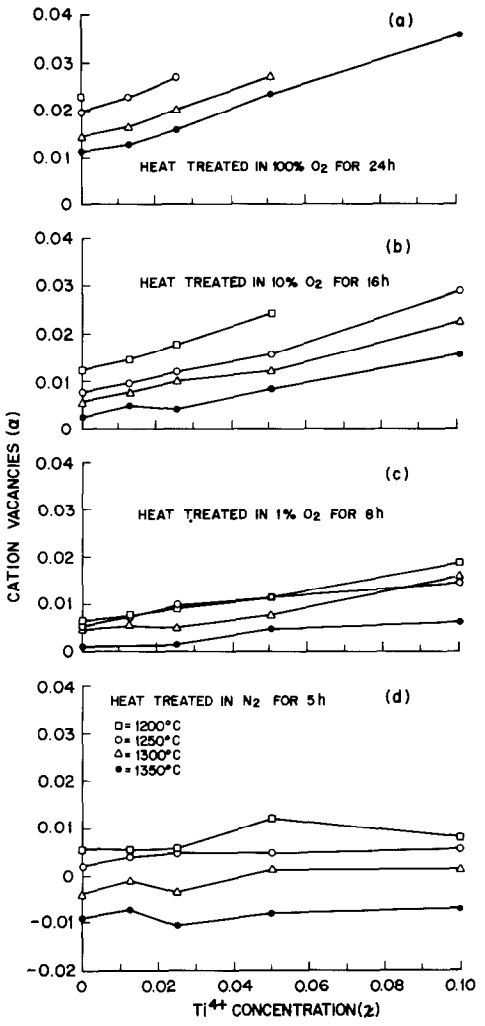

FIG. 2. Cation vacancies vs Ti^{4+} added (both expressed as $M_3Ti_x^{4+}V_\alpha O_{4+\beta}$) for various heat treatments.

divalent iron which lead to the negative α values through the calculations came in part from Zn loss at the highest temperatures. Zinc has an increasing tendency to vaporize at high temperature as the atmosphere becomes reducing because it vaporizes by a dissociative mechanism. This loss is expected to be compensated by the reduction of some iron, assuming that some of the cation vacancies formed will be offset by reduction of Fe^{3+}.

The rate at which vacancies are formed in the structure as Ti^{4+} is added can be deduced from the slopes of the lines in Fig. 2. From Fig. 2 it can be seen that while there is some scatter to the data, the vacancy content is approximately a linear function of the Ti^{4+} content. By smoothing the data to straight lines one can measure the slopes to give the approximate relationship between α and x. The slopes, $d\alpha/dx$, range from about 0 to 0.3 vacancies per Ti^{4+} added. This can be compared to the limiting cases in Eqs. (1) and (2). For Eq. (1), the slope would be 0.5 with the addition of Ti^{4+}, resulting in the formation of vacancies with no reduction of Fe^{3+} to Fe^{2+}, and for Eq. (2) the slope would be 0.0 with all of the Ti^{4+} being charge compensated by reduction of iron with no vacancies being formed.

As expected, the actual values of $d\alpha/dx$ fall between the limiting cases described above. However, within the ranges observed, there is a relationship between the slope $d\alpha/dx$ and the degree of oxidation of the structure with no Ti^{4+} added. This relationship is shown in Fig. 3 where $d\alpha/dx$ is plotted as a function of α_0, the vacancy content with no Ti^{4+} added. The slopes are those of least-squares straight lines through the data in Fig. 2 with the two data points excluded for the

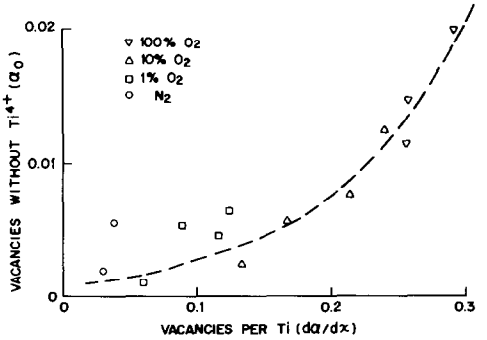

FIG. 3. Cation vacancy contents with no Ti^{4+} vs vacancies per Ti^{4+} added (slopes of lines in Fig. 2). Broken curve shows trend and can be used for estimating the vacancy content of Ti^{4+}-substituted MnZn ferrites.

samples fired in N_2 which showed negative α_0 due to Zn loss.

Figure 3 shows the potency of Ti^{4+} for inducing vacancies as a function of the overall oxygen content of the ferrite. The oxygen content is represented as the vacancy content for that composition and heat treatment without Ti^{4+}. The data points in Fig. 3 represent the four firing atmospheres as well as differing temperatures for each atmosphere. It can be seen that those conditions which induce vacancies without Ti, namely, higher p_{O_2} and lower temperatures, also render any Ti dopant even more potent in forming further vacancies. On the other hand, as the firing conditions became sufficiently reducing, the ferrite is nearly stoichiometric and the tendency of additions of Ti^{4+} to increase the vacancy content becomes small. This is not surprising since in spinel ferrites cation vacancies are common, but there is much less tendency to form anion vacancies. Thus, for ferrites fired in relatively nonoxidizing conditions, the cation vacancy content will be near zero and additions of Ti^{4+} serve only to allow reduction of Fe^{3+} without introducing energetically unfavorable anion vacancies. This leads to only small increases in the vacancy content. The ineffectiveness of Ti in producing vacancies for nonoxidizing conditions further suggests that the results of Hanke (*19*), where substitutions of Ti^{4+} for Mn^{2+} or Zn^{2+} lead only to the formation of Fe^{2+} with negligible increases in the cation vacancy concentration, were obtained for samples heat treated under such nonoxidizing conditions.

Differentiating Eq. (5),

$$\frac{dk}{dx} = \frac{4}{3} - \frac{8}{3}\frac{d\alpha}{dx}. \tag{6}$$

This, of course, shows that for addition of Ti^{4+} to ferrites fired in nonoxidizing conditions ($d\alpha/dx \cong 0$) the rate change of excess Fe^{2+} content with Ti^{4+}, $dk/dx \cong \frac{4}{3}$. However, under the conditions which are the most oxidizing without forming a second phase $d\alpha/dx \cong 0.3$ and $dk/dx \cong 0.5$. Thus, if the vacancy content (or Fe^{2+} content) of a ferrite is known in the undoped condition, one can predict the rate of change of $d\alpha/dx$ and dk/dx using the data in Fig. 3, and then, in turn, predict the degree of oxidation of the ferrite at any Ti^{4+} concentration for those firing conditions. Again, the reader is referred to the work of Morineau (*18*) for a discussion of the role of Mn^{3+} in ferrites since the presence of Mn^{3+} would add to the actual Fe^{2+} in the solid state.

While this work provides a complete data set for the effect of the variables temperature, p_{O_2}, and Ti^{4+} dopant levels, it is restricted to a single MnZn ferrite composition. The concepts presented here can be extended by using the charts provided by Morineau and Paulus (*29*) which give the oxygen content of MnZn ferrites as a function of T, p_{O_2}, as well as composition. From these data, the vacancy content with no additions can be calculated and, except for large deviations of composition from that used in this study, the data in Fig. 3 are useful for estimating the effect of Ti^{4+} on the stoichiometry.

(*b*) *Phase Equilibria*

As mentioned earlier, the addition of Ti to the MnZn ferrite resulted in the formation of two phases at high p_{O_2} and low temperatures. Figure 4 shows an area heavily covered with this precipitate. The stabilization of a hexagonal hematite-like phase relative to a magnetic spinel by TiO_2 has been reported by MacChesney and Muan (*30*). Similarly, the addition of TiO_2 to MnZn ferrite stabilizes a hexagonal hematite-like structure. The phase boundary between the single-phase spinel region and the two-phase region can be determined using microscopy or by noting the composition at which the Fe^{2+} content begins to decrease with increasing Ti^{4+}. Figure 1 shows an example of decreasing Fe^{2+} with precipitation. Figure 5 shows the phase boundary for this ferrite using both the microstructural and divalent iron studies

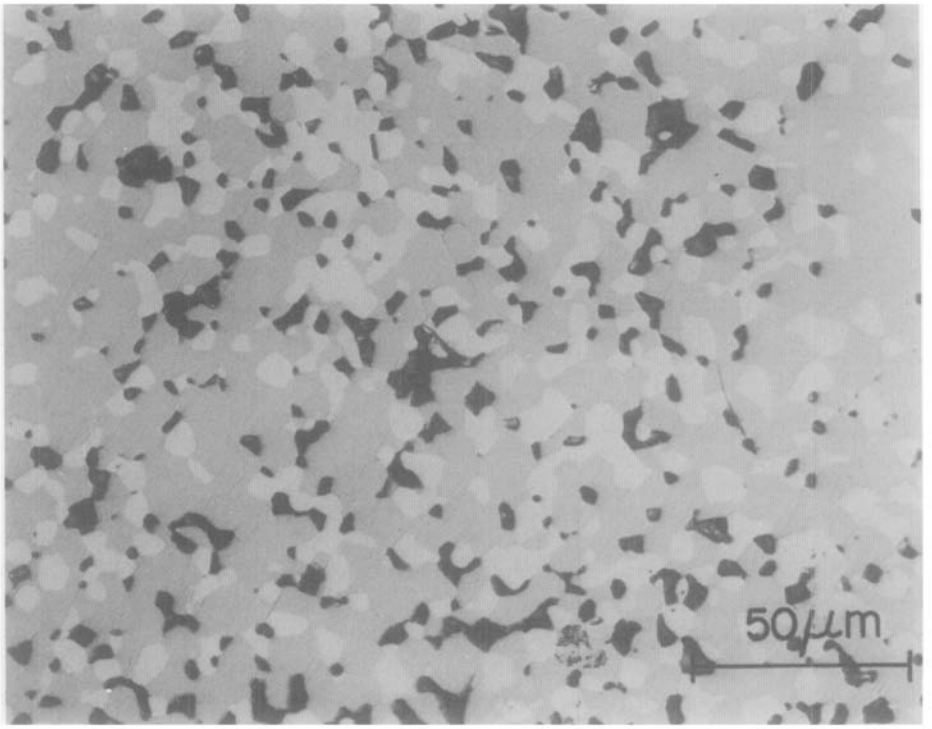

FIG. 4. Typical micrograph of the ferrite with Ti level of $x = 0.10$ heat treated at 1200°C in O_2 showing the dark pore phase, the intermediate spinel phase, and the light hexagonal hematite-like phase.

for definition. The position of the phase boundary is in excellent agreement with that from other work (*31*) where the samples were not quenched.

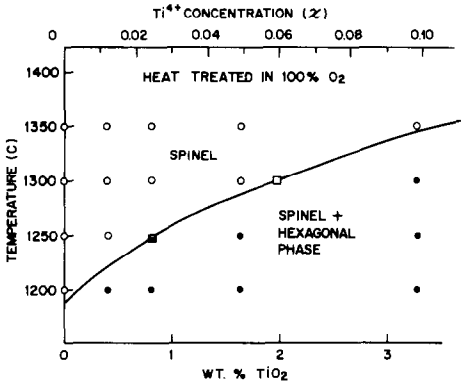

FIG. 5. Phase boundary showing the stabilization of the hexagonal phase with TiO_2 additions. The closed and open circles show the presence or absence of the hexagonal phase by microscopy. The square data points were taken from the point of slope change in the Fe^{2+} contents in Fig. 1.

Using the phase boundary in Fig. 5, the Ti contents at the phase boundaries can be found for the temperatures at which data were taken. These data, in turn, can be used with Fig. 2a to calculate the concentration of vacancies at the phase boundary. In this case extrapolations of the slopes of $d\alpha/dx$ in the single-phase region were used to determine critical vacancy contents (α_c) at which precipitation occurs. These data are plotted in Fig. 6 to show the temperature dependence of α_c. At 1200°C there are two data points since the phase boundary was observed at both 100 and 10% O_2. Also shown in Fig. 6 are the vacancy contents at the phase boundary as calculated from data published by Slick (*16*) and Morineau and Paulus (*17*). The indicated data points were calculated from the published data using the reported stoichiometry of the ferrites where the lines of constant oxygen content meet the phase boundary. Note that while the data in Fig. 6

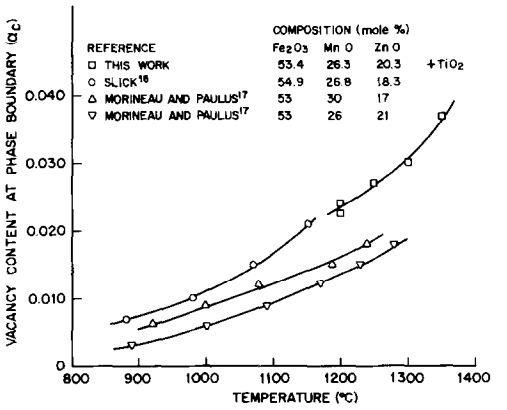

FIG. 6. Comparison of vacancy contents at the phase boundary using Ti^{4+}-substituted MnZn ferrites for this work with those calculated from literature data on undoped ferrites.

taken from this work resulted primarily from changing Ti^{4+} content with a constant firing atmosphere and that from the literature resulted from varying the atmosphere with no Ti, the data sets are in reasonable agreement. Thus the precipitation of hematite from ferrite under oxidizing conditions can be more generally viewed as occurring when the spinel becomes saturated with vacancies. The vacancies can be formed by oxidizing heat treatments or by additives such as TiO_2, but the saturation vacancy content (α_c) depends primarily on temperature.

There is some indication that the maximum vacancy content in MnZn ferrite is less than that tolerated by some other spinel systems. For instance, Taylor (*32*) found that over the complete solid solution series between magnetite and $TiFe_2O_4$, the maximum vacancy content was 2% of the cation sites ($\alpha_c = 0.06$) at 1300°C. This concentration of vacancies in the end member, magnetite, is in agreement with that reported by Darken and Gurry (*33*) and by Dieckmann and Schmalzried (*34*).

(*c*) *Compositional Studies in the Two-Phase Region*

Initial X-ray diffraction studies showed the second phase to be the expected hematite-like hexagonal material. The composition with the maximum Ti^{4+} ($x = 0.10$) fired at the highest p_{O_2} (100%) and lowest temperature (1200°C) showed, of course, the greatest amount of the hexagonal phase and therefore was studied more deeply. It was estimated from the relative intensities of the diffraction peaks that about 20% of the sample was the hexagonal phase. Attempts were made to ascertain the composition of this phase by noting the displacement of the *d* spacings from that of α-Fe_2O_3. However, not only $FeTiO_3$ but also $MnTiO_3$ and perhaps $ZnTiO_3$ are soluble in Fe_2O_3. Thus, lattice spacing data alone cannot characterize the composition of the hexagonal phase.

The volume fraction of each phase was determined from point counts on optical micrographs and the elemental composition of each phase was determined by electron microprobe. The hexagonal and spinel phases were clearly visible on scanning images (Fig. 7), and point by point measurements across the central regions showed the composition to be uniform. Quantitative determinations were made by taking intensity ratios of unknowns to pure standards and using MAGIC (*35*) for data reduction. All data were taken at 20 keV excitation voltage with counting times of 100 sec. Four different areas were sampled for each phase and quantitative values were averaged. Two σ limits were less than ±3% except in cases of very low concentrations. The combined results of the volume fraction measurements and chemical analyses for Ti contents of $x = 0.0125$ and 0.10 fired at 1200°C in O_2 are shown in Table I. The hexagonal phases are listed such that the sum of the metal ions equals 2 (as in Fe_2O_3).

With the data in Table I and the total chemical analyses giving the total cation ratios as $Mn_{0.515}Zn_{0.397}Fe_{2.089}Ti_x$, the composition of the system is overdetermined in the sense that any two of the analyses can be used as a verification check on the third. Furthermore, if one assumes no vacancies in the hexagonal phase, the Fe^{2+} data can be

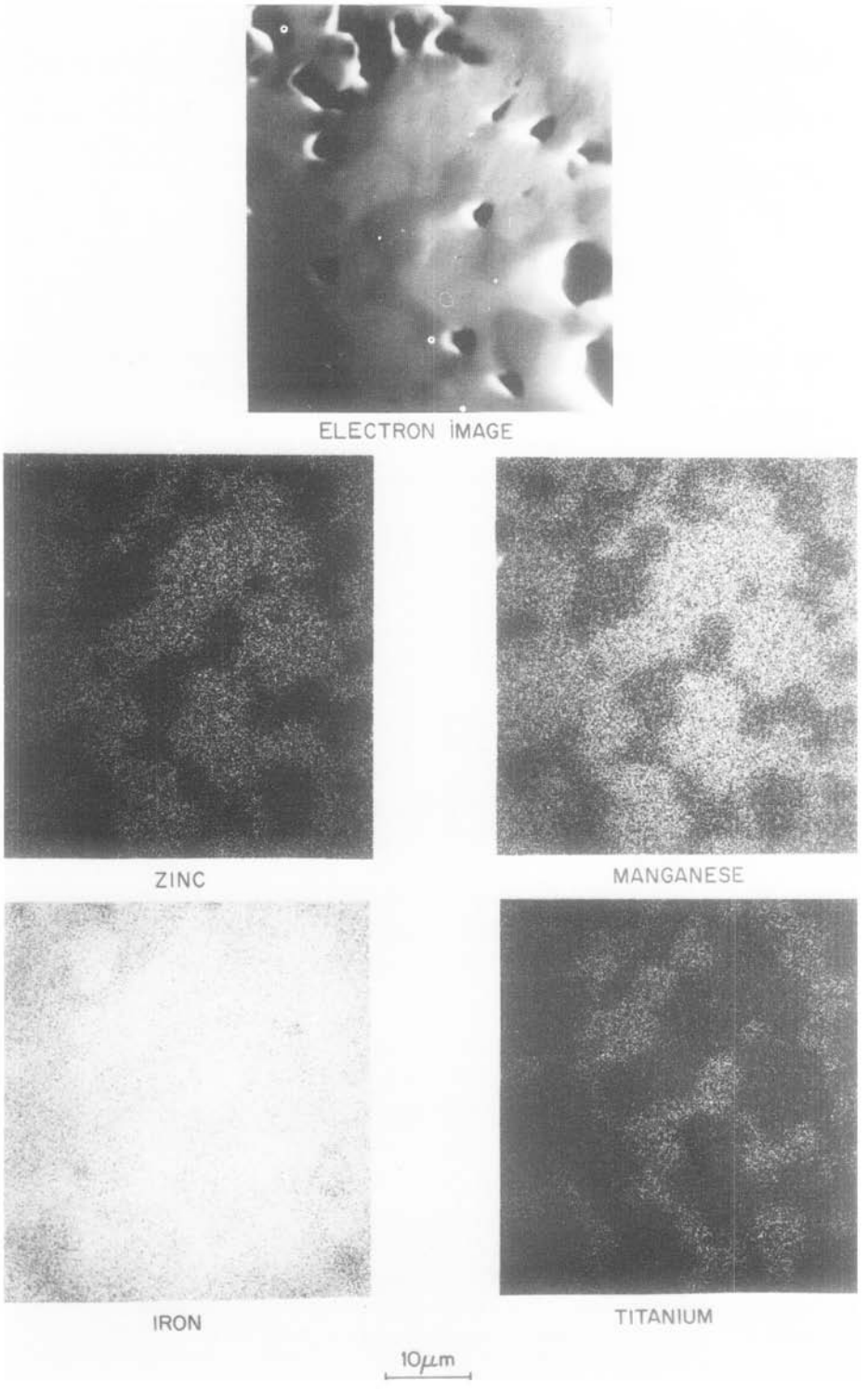

FIG. 7. Electron and elemental characteristic X-ray images of ferrite with Ti level of $x = 0.10$ heat treated at 1200°C in O_2 showing concentration of Fe and Ti in the hexagonal second phase.

TABLE I

MEASURED METAL RATIOS AND RELATIVE VOLUME FRACTIONS OF HEXAGONAL AND SPINEL PHASES (1200°C IN O_2)

Total Ti^{4+} (x)	Hexagonal phase (M_2O_3)					Spinel phase (M_3O_4)				
	Fe	Mn	Zn	Ti	Vol %	Mn	Zn	Fe	Ti	Vol %
0.0125	1.788	0.117	0.031	0.065	4	0.530	0.394	2.075	0.010	96
0.10	1.579	0.174	0.075	0.173	24	0.592	0.470	1.939	0.056	76

used to calculate the amount of Fe^{2+} and the vacancy content of the spinel phase. To do these calculations, the total composition was taken to be the most reliable because it was done on macroscopic samples. The composition of the hexagonal phase was taken from the microprobe data (Table I) and subtracted according to the volume fraction present from the total composition. The remaining calculated spinel composition can then be compared to that measured by the electron microprobe.

The results of these calculations are shown in Table II for the two Ti^{4+} contents studied by microprobe. For the hexagonal phases, the valances of the Mn ions (from Table I) were set such that the Mn^{2+} and Zn^{2+} contents were equivalent to the Ti^{4+} content while all the Fe is trivalent (assumes negligible lattice defects for the hexagonal phase). The composition of the hexagonal phase was normalized to the same molecular weight as the total composition and the appropriate fraction of the hexagonal phase (vol% hexagonal phase in Table I with the densities of both phases assumed to be equal) was subtracted from the total composition to give the calculated spinel composition. At the same time, the divalent iron analyses data (Fig. 1) were used to calculate the amount of divalent iron and thus the vacancy concentration for the spinel phase since the oxidation states of the ions in the hexagonal phase were fixed. Again, the notation is such that there is no Mn^{3+} in the presence of Fe^{2+}.

It can be seen in Table II that there is excellent agreement between the calculated and measured spinel compositions. Note that both Ti and Fe concentrate in the hexagonal phase. This can also be observed in Fig. 7 by comparing the imaged displays of the X-ray analyzers. At high doping levels, no divalent

TABLE II

CALCULATED SPINEL COMPOSITIONS (1200°C IN O_2)

Total Ti^{4+} (x)	Phase	Composition measurement technique	Mn^{2+}	Mn^{3+}	Zn^{2+}	Fe^{2+}	Fe^{3+}	Ti^{4+}	Vacancies (α)
0.0125	Hexagonal	Microprobe	0.034	0.083	0.031	—[a]	1.788	0.065	—[a]
0.0125	Spinel	Total − Hexagonal	0.526	—[a]	0.412	0.018	2.044	0.009	0.021
0.0125	Spinel	Microprobe	0.530		0.394	2.075		0.010	—
0.100	Hexagonal	Microprobe	0.098	0.076	0.075	—[a]	1.579	0.173	—[a]
0.100	Spinel	Total − Hexagonal	0.560	0.019	0.478	—[a]	1.944	0.047	0.009
0.100	Spinel	Microprobe	0.592		0.470	1.939		0.056	—

[a] Based on model of negligible vacancies and Fe^{2+} in the hexagonal phase.

iron exists and, in fact, the negative values of the Fe^{2+} content seen in Fig. 1 (measured by back-titrating additions of ferrous sulfate) are indicative of Mn^{3+}. Finally, the calculated vacancy contents should fall on the curves in Fig. 6 since the two phases were in equilibrium at 1200°C. Indeed, for the $x = 0.0125$ sample, the α_c of 0.021 is close to the other data points at 1200°C for this work. However, for the $x = 0.1$ sample, the α_c of 0.009 is considerably lower than expected. This is most likely an error due to the inaccuracy of the technique for measuring volume percentage of second phase. Small errors in measurement of the percentage second phase make large errors in the calculated vacancy content and therefore the calculated vacancy contents in Table II are not reliable. For example, for $x = 0.10$, if the amount of hexagonal phase were 21% (close to that predicted from X-ray diffraction) rather than 24%, then the calculated α_c would be about 0.023 as predicted from Fig. 6. An error of this magnitude in the volume percentage of hexagonal phase is quite possible.

Conclusions

1. For single-phase MnZn ferrite spinel, increasing the amount of Ti^{4+} leads to increases in the Fe^{2+} content and cation vacancies. The increase in vacancies is approximately linear with Ti^{4+} content and the slope $d\alpha/dx$ is between about 0 and 0.3 depending on the firing conditions. Data are presented relating $d\alpha/dx$ to the vacancy content in an undoped ferrite in any firing conditions.

2. Ti^{4+} in ferrite will stabilize the hexagonal hematite-like structure. The phase boundary between the single- and two-phase regions as a function of Ti^{4+} content and temperature is presented. The relationship between the initial vacancy content at the phase boundary was calculated for data taken from samples fired in 100% O_2 with varying Ti^{4+} contents and was in good agreement with that calculated from the literature when the atmosphere was varied with no dopants.

3. The hexagonal phase contains Mn, Zn, and Ti as well as Fe with a disproportionate amount of Ti and Fe residing in the hexagonal rather than the spinel phase. The compositions and proportions of the hexagonal and spinel phases are self-consistent.

Acknowledgments

The authors wish to thank E. M. Vogel for valuable assistance in sample preparation and characterization and F. Schrey for the Coprex analyses.

References

1. B. B. GHATE, *in* "Processing of Crystalline Ceramics," (H. Palmour, III, R. F. Davis and T. M. Hare, eds.), p. 369, Plenum Press, New York (1978).
2. T. G. W. STIJNTJES, J. KLERK, AND A. BROESE VAN GROENOU, *Philips Res. Rep.* **25**, 95 (1970).
3. E. RÖSS AND I. HANKE, *Phys. Status Solidi A* **2**, K185 (1970).
4. T. G. W. STIJNTJES AND J. KLERK, *in* "Ferrites: Proceedings, International Conference, July 1970" (Y. Hoshino, S. Iida, and M. Sugimoto, eds.), p. 191, Univ. of Tokyo Press, Tokyo (1971).
5. T. G. W. STIJNTJES, A. BROESE VAN GROENOU, R. F. PEARSON, J. E. KNOWLES, AND P. RANKIN, *in* "Ferrites: Proceedings, International Conference, July 1970" (Y. Hoshino, S. Iida, and M. Sugimoto, Eds.), p. 194, Univ. of Tokyo Press, Tokyo (1971).
6. B. HOEKSTRA AND V. A. M. BRABERS, *Solid State Commun.* **17**, 249 (1975).
7. M. F. YAN AND D. W. JOHNSON, JR., *J. Amer. Ceram. Soc.* **61**, 343 (1978).
8. A. FOX, *J. Phys. D* **4**, 1239 (1971).
9. S. OGAWA, T. NAKAJIMA, T. SASAKI, AND M. TAKAHASHI, *Japan. J. Appl. Phys.* **7**, 899 (1968).
10. S. IIDA, *J. Phys. Soc. Japan* **17**, 123 (1962).
11. J. E. KNOWLES, *Philips Res. Rep.* **29**, 93 (1974).
12. I. C. HECK, "Magnetic Materials and Their Applications" (S. Hill, Transl.), p. 63, Crane, Russak & Co., New York (1974).
13. C. O'HARE, R. KENWORTH, AND R. C. WHITEHEAD, *Proc. Brit. Ceram. Soc.* **10**, 245 (1968).

14. T. MATSUBARA, J. KAWAI, AND I. SUGANO, *in* "Ferrites: Proceedings, International Conference, July 1970" (Y. Hoshino, S. Iida, and M. Suginomoto, Eds.), p. 191, Univ. of Tokyo Press, Tokyo (1971).
15. S. IIDA, *in* "Ferrites: Proceedings, International Conference, July 1970" (Y. Hoshino, S. Iida, and M. Sugimoto, Eds.), p. 17, Univ. of Tokyo Press, Tokyo (1971).
16. P. I. SLICK, *in* "Ferrites: Proceedings, International Conference, July 1970" (Y. Hoshino, S. Iida, and M. Sugimoto, Eds.), p. 81, Univ. of Tokyo Press, Tokyo (1971).
17. R. MORINEAU AND M. PAULUS, *Phys. Status Solidi A* **20**, 373 (1973).
18. R. MORINEAU, *Phys. Status Solidi A* **38**, 559 (1976).
19. I. HANKE, *Ber. Deut. Keram. Ges.* **49**, 295 (1972).
20. I. HANKE AND M. ZENGER, *J. Magnetism Magn. Mater.* **4**, 120 (1977).
21. W. M. LATIMER, "Oxidation Potentials," 2nd ed., Prentice–Hall, Englewood Cliffs, N.J. (1952).
22. F. K. LOTGERING AND A. M. VAN DIEPEN, *J. Phys. Chem. Solids* **34**, 1369 (1973).
23. M. SUGAMOTO, *in* "Sintering and Related Phenomena" (G. C. Kuczynski, N. A. Hooton, and C. F. Gibbon, Eds.), p. 759, Gordon and Breach, New York (1967).
24. F. WALZ AND J. RIVAS, *Phys. Status Solidi A* **37**, 151 (1976).
25. F. SCHREY AND P. K. GALLAGHER, *Amer. Ceram. Soc. Bull.* **56**, 981 (1977).
26. F. J. SCHNETTLER, F. R. MONFORTE, AND W. W. RHODES, *in* "Science of Ceramics" (G. H. Stewart, Ed.), Vol. 4, p. 79. The British Ceramic Society, Stoke-on-Trent (1968).
27. P. K. GALLAGHER, *Amer. Ceram. Soc. Bull.* **57**, 576 (1978).
28. E. E. UNDERWOOD, "Quantitative Stereology," p. 25, Addison–Wesley, Reading, Mass. (1970).
29. R. MORINEAU AND M. PAULUS, *IEEE Trans. Magn.* **Mag-11**, 1312 (1975).
30. J. B. MACCHESNEY AND A. MUAN, *Amer. Mineral.* **44**, 926 (1959).
31. M. F. YAN AND D. W. JOHNSON, JR., *in* "Processing of Crystalline Ceramics," (H. Palmour, III, R. F. Davis and T. M. Hare, eds.), p. 393, Plenum Press, New York (1978).
32. R. W. TAYLOR, *Amer. Mineral.* **49**, 1016 (1964).
33. L. S. DARKEN AND R. W. GURRY, *J. Amer. Chem. Soc.* **68**, 798 (1946).
34. R. DIECKMANN AND H. SCHMELZRIED, *Ber. Bunsenges. Phys. Chem.* **81**, 344 (1977).
35. J. W. COLBY, *in* "Proceedings, Sixth National Conference on Electron Probe Analysis," paper No 17, Electron Probe Analysis Society (1971).